Interfacial strength and microstructure of AlN/Cu joints produced by a novel brazing method facilitated by porous-copper layer and Ag foil

Yilian Huang
Nanjing University of Aeronautics and Astronautics College of Material Science & Technology
Renli Fu (renlifu@nuaa.edu.cn)
Nanjing University of Aeronautics and Astronautics https://orcid.org/0000-0001-6449-7974
Xudong Chen
Nanjing University of Aeronautics and Astronautics College of Material Science & Technology
Bo Cheng
Nanjing University of Aeronautics and Astronautics College of Material Science & Technology
Simeon Agathopoulos
University of Ioannina Department of Materials Science and Engineering: Panepistemio Ioanninon Tmema Mechanikon Epistemes Ylikon

Research Article

Keywords: AlN ceramic, brazing, shear strength, microstructure, reaction mechanism

Posted Date: March 22nd, 2021

DOI: https://doi.org/10.21203/rs.3.rs-345413/v1

Abstract

The reliability of wide-bandgap (WBG) semiconductors used as power electronics is closely related to the high thermal conductivity of AlN-metalized substrates. Thus, the bonding of AlN ceramics with metals is a key issue for the production of reliable AlN-metalized substrates. This paper reports on a new method for producing AlN/Cu joints by employing a novel film-metallization production process, which involves a porous network of Cu layer and Ag foil. The microstructure and the phases formed at the interface of the AlN/Cu joints produced at various brazing temperatures and times, were analyzed by scanning electron microscopy and X-ray diffraction analysis. Strong joints with shear strength of 48.5 MPa were produced after brazing at 850 °C for 10 min. The typical microstructure at the interfacial reaction zone was Cu / Ag(s) + Cu(s) / $CuAlO_2$ + Al_2O_3 + Cu(s) / AlN. The experimental results manifest the crucial role of the Ag-Cu eutectic liquid phase, formed by the reaction between the Cu layer and the Ag foil, and of the porous network of the Cu layer deposited on the surface of the AlN ceramic substrate, since both of them effectively favor the reduction of the residual thermal stresses in the joint and result in strong ceramic/metal joins.

1. Introduction

Electronics aimed at power applications are being rapidly developed nowadays. Hence, wide-bandgap (WBG) semiconductors attract growing interest in the fields of renewable energy sources [1], high-speed railways [2], aircrafts [3], electric vehicles [4], space exploration [5], etc. Compared to traditional silicon (Si) devices, the WBG semiconductors exhibit excellent performance at higher temperatures and withstand higher current densities, resulting in superior power conversion with higher efficiency and compact volume, in conjunction with lower energy consumption [6–8]. Nonetheless, the WBG semiconductor devices increase their internal temperature cyclically because of the heat produced during operation [5]. The feature of high thermal conductivity of metalized-ceramic substrates is an important issue directly linked to the high reliability of WBG power electronics [8].

Metalized-ceramic substrates display high current-carrying capability and the coefficient of their thermal expansion (CTE) is close to the CTE of silicon. Consequently, they are suitable for power-electronic applications [9]. Direct-bond copper (DBC) technology is usually applied for ceramic metallization, since copper can develop a strong interfacial bond with ceramics. Alumina is the most commonly used ceramic due to good thermal conductivity (24.7 $Wm^{-1}{\cdot}K^{-1}$), low CTE ($6.5{\times}10^{-6}$ K^{-1}), and low cost [10]. However, its thermal conductivity is insufficient for power electronics with a wide bandgap [5]. On the other hand, aluminum nitride (AlN) ceramic demonstrates higher thermal conductivity (70–210 $Wm^{-1}{\cdot}K^{-1}$ for the polycrystalline AlN) and lower CTE (4.4×10^{-6} K^{-1}) than alumina, yet close to the values of silicon [8]. Accordingly, AlN metalized-ceramic substrates are very promising for WBG power-electronic packaging [9].

Most metal materials feature low self-diffusion coefficient and poor wettability. Therefore, metallization of AlN ceramics is difficult. Furthermore, the mismatch between the CTE of AlN and the metal layers leads

to development of thermal stresses at the ceramic/metal interface after cooling the joint from the high-bonding temperature to room temperature [11]. Two methods are applied to join copper to AlN ceramic, termed as direct-bond copper (DBC) and active-metal bonding (AMB) [12, 13].

The method of DBC relies on the Cu-Cu_2O eutectic liquid between copper and the oxide of Cu_2O on the surface of the ceramic, whereby ceramic/metal joining can successfully occur [14]. Nevertheless, the Cu-Cu_2O eutectic liquid is hardly formed between AlN ceramic and copper, ascribed to the insufficient amount of oxide on the surface of AlN ceramic [15]. Thus, in order to join AlN to copper by DBC method, oxygen must be provided on the surface of AlN ceramics to produce a thin layer of Al_2O_3, needed to join the two aforementioned materials [16]. Nevertheless, the presence of Al_2O_3 interlayer will deteriorate the thermal conductivity of AlN (the thermal conductivity of AlN is more than 10 times higher than that of Al_2O_3) [17]. Moreover, owing to the CTE mismatch among copper, Al_2O_3, and AlN, microcracks in the alumina layer may be formed, thereby the reliability of the substrate is reduced [18, 19].

The method of AMB is based on the reaction of active metals (such as Ti, Zr, V, etc.) with ceramics [20], whereby the interfacial metal compound formed between the ceramic and the metal facilitates the ceramic/metal joining [21, 22]. In comparison with the DBC method, the product of AlN bonded to Cu by the AMB method exhibits smaller thermal resistance and less porosity at the interface [23]. However, the problem of the CTE mismatch between AlN and Cu still exists. Hence, a brazing alloy with low CTE can be used in order to reduce the detrimental thermal stresses in the ceramic/metal interface [24, 25]. Nonetheless, the brazing fillers used in the AMB method are of high cost, which is a serious issue in the production process of AlN/Cu composites on a large industrial scale.

Consequently, the development of a method for joining aluminum nitride and copper through a low-temperature, pressureless, and simple process is an urgent demand in industrial applications. This paper reports on the development of a novel method to join AlN ceramics to copper with the aid of Ag foil. In brief, a porous-mesh copper layer was deposited on the surface of AlN ceramic. Then, a silver foil was employed, as a brazing filler, to join the AlN ceramic to copper. The features of the interfacial reaction zone of the ceramic/metal joint were thoroughly analyzed and the bonding strength was experimentally measured. A mechanism of the evolution of the AlN/Cu interfacial microstructure is proposed.

2. Materials And Experimental Procedure

AlN-ceramic substrates (1 mm, > 99%, Fujian Huaqing Electronic Material Technology Co., Ltd., China), copper pillars (Ø2 × 1 mm, > 99 %, Shenzhen Tianfa Metal Material Co., Ltd., China), oxygen-free highly-conductive copper foil (OFHC, 0.2 mm, > 99 %, Sinopharm Chemical Reagent Co., Ltd., China), CuO nano-powder (100 nm, > 99%, Sinopharm Chemical Reagent Co., Ltd., China), and Ag foil (0.02 mm, > 99 %, Sinopharm Chemical Reagent Co., Ltd., China) were used. The AlN ceramic, the OFHC copper foil, and the Ag foil were tailored to rectangular samples in the size of (in mm) 8 × 8 × 1, 8 × 8 × 0.20, and 8 × 8 × 0.02, respectively. The surface of the copper foils, the copper pillars, and the AlN ceramics were coarsely ground, polished, and finally ultrasonically cleaned for 20 min in a distilled water bath prior to brazing.

The CuO nanoparticles were granulated with the aid of organic binders by mechanical means to form a homogeneous CuO paste.

The novel method for bonding the AlN ceramics with copper is schematically presented in Fig. 1a. The process comprises three stages. (1) A film of CuO paste, with a thickness of 100–110 μm, was deposited on the surface of the AlN substrate by screen printing. Sintering at 1075 ^{o}C in air for 30 min followed. (2) The CuO-coated AlN substrates were heat-treated at 400 ^{o}C for 2 h under reduction atmosphere (N_2 – 20% H_2) in order to reduce the CuO film and to form a porous-copper layer on the AlN ceramic. (3) An assembly of copper plate/copper pillar and Ag foil was put onto the surface of the AlN substrate, as schematically illustrated in Fig. 1b. Subsequently the assemblies were placed in a vacuum furnace (NBD-103, Zhengzhou, Nobady Material Technology Co., Ltd., China) for brazing under vacuum of $< 2 \times 10^{-3}$ Pa. The melting temperature of Ag-Cu eutectic is 780 ^{o}C. In order to study the influence of temperature, the brazing temperature was selected to be in the range of 810–860 ^{o}C. Experiments were also performed at 785 ^{o}C for several times (0–20 min).

The morphology of the surface of the metalized ceramic, as well as the fracture surface and cross-sections of the prepared ceramic/metal joints, was observed by scanning electron microscopy (SEM, LYRA3, TESCAN, Czech Republic). The CuO film and the porous copper layer on the AlN substrate produced in the processes (1) and (2) (Fig. 1) were removed by 20 wt% HCl alcohol solution and 10 wt% $FeCl_3$ solution, in order to analyze the ceramic phases at the interface between AlN and CuO or Cu. The crystallographic analysis of the phases developed at the interfaces was performed by X-ray diffraction analysis (XRD, D8 Advance, Bruker, Germany) with Cu K_{α} radiation. The shear strength of the produced joints was measured by a push-tension tester (STR 1000, Rhesca, Japan) at room temperature.

3. Results And Discussion

3.1 Microstructure of the copper surface layer produced by the reduction of CuO

The morphology of the CuO layer and the reduced-Cu layer deposited on the surface of the AlN-ceramic substrate by the thick-film method is depicted in Fig. 2. The CuO layer features a porous coral-like structure (Fig. 2a). There are pores on micro-scale among the CuO grains. The reduced Cu layer has maintained the porous structure of the CuO layer (Fig. 2c). Compared to the CuO layer (Fig. 2b), there are many nano-pores in the Cu layer, as well (Fig. 2d). The cross-section of the CuO and the Cu layers deposited on the AlN-ceramic substrate is shown in Fig. 3. The CuO layer has a coral-like porous-network structure (Fig. 3a). The reduced Cu layer retains this porous-network structure of CuO. Nano-pores are also observed to be uniformly distributed in the Cu layer (Fig. 3b).

The crystalline phases developed in the above microstructures were detected by X-ray diffraction analysis (Fig. 4). More specifically, after sintering at 1075 ^{o}C for 30 min, the CuO layer is mainly composed of CuO and Cu_2O (bottom diffractogram in Fig. 4a). After the reduction under N_2-H_2 atmosphere, these oxides

(CuO and Cu_2O) are reduced to Cu, as plotted in the upper diffractogram in Fig. 4a. Then, both samples were subjected to chemical etching. The X-ray diffractograms from the surface of these samples (i.e. the surface of the AlN-ceramic samples after chemical etching) are shown in Fig. 4b. The AlN/CuO interface is mainly composed of $CuAl_2O_4$, $CuAlO_2$, and a small amount of Al_2O_3, (bottom diffractogram). The AlN/Cu interface consists chiefly of $CuAlO_2$ and a small amount of Al_2O_3, (upper diffractogram). Some very small peaks were assigned to traces of $YAlO_3$, which inevitably exist in the parent AlN ceramic.

The following lines aim to shed light on the development of these phases. According to the Cu-O phase diagram, CuO should be decomposed into O_2 and Cu_2O during sintering at 1075 ^oC [26]:

$$4\ CuO \rightarrow 2\ Cu_2O + O_2 \uparrow \quad (1)$$

The O_2 produced by the chemical reaction represented by the chemical equation (1) can be diffused in the interface of AlN/CuO and reacts with AlN to form Al_2O_3 and N_2:

$$4\ AlN + 3\ O_2 \rightarrow 2\ Al_2O_3 + 2\ N_2 \uparrow \quad (2)$$

Then, the N_2 diffuses in the air through the AlN/CuO interface and forms channels into the CuO layer, resulting in the coral-like porous-network structure (Fig. 3a).

Cu_2O and Al_2O_3, which are the products of the reaction represented by the chemical equations (1) and (2), react at the interface of AlN/CuO to form $CuAlO_2$ [27]. Meanwhile, the non-decomposed CuO can also react with Al_2O_3 to form $CuAl_2O_4$. In addition, $CuAl_2O_4$ can also be produced from $CuAlO_2$ when O_2 is sufficient [28]. These reactions are represented by the following chemical equations:

$$Cu_2O + Al_2O_3 \rightarrow 2\ CuAlO_2 \quad (3)$$

$$CuO + Al_2O_3 \rightarrow CuAl_2O_4 \quad (4)$$

$$4\ CuAlO_2 + 2\ Al_2O_3 + O_2 \rightarrow 4\ CuAl_2O_4 \quad (5)$$

During the reduction process, H_2 can enter the CuO layer through the channels produced during the sintering process. Accordingly, reduction of the phases of CuO and Cu_2O can occur:

$$CuO + H_2 \rightarrow Cu + H_2O \uparrow \quad (6)$$

$$Cu_2O + H_2 \rightarrow 2\ Cu + H_2O \uparrow \quad (7)$$

The phase of $CuAlO_2$ (Fig. 4b) can be formed through the reaction described by the following chemical equation [29]:

$$2\ CuAl_2O_4 + H_2 \rightarrow 2\ CuAlO_2 + Al_2O_3 + H_2O \uparrow \quad (8)$$

According to this reaction, the discharging of water (H_2O) steam leads to the formation of the fine nano-pores in the Cu layer, shown in Figs. 2d and 3b.

3.2 Bond strength and interfacial microstructure of AlN/Cu joints

The average values of the shear strength of the AlN/Cu joints produced after brazing for 10 min at various temperatures are presented in the plot of Fig. 5. The shear strength increases when the temperature rises and a maximum of 48.5 MPa was recorded for the joint produced at 850 ^{o}C. Heat-treatment at higher temperatures resulted in a decrease of the interfacial strength.

The joint strength is directly linked to the features of the developed ceramic/metal interface. Typical images from fractography of AlN/Cu joints are illustrated in Fig. 6. The fracture occurs at the interface between the ceramic and the brazing-filler metal. With the increase of brazing temperature, a gradual, inward extension of the cracks towards the side of the ceramic, is observed. In the samples produced at 850 ^{o}C, all the cracks appear on the ceramic side, and a typical arch-shaped fracture is observed (Fig. 6e). These results support the increase of bonding strength of the AlN/Cu joints with the increase of the brazing temperature (Fig. 5).

When the brazing temperature is increased further (>850 ^{o}C), the arched-shaped fracture morphology is still observed but deeper cracks are propagated through the AlN ceramic, as depicted in Fig. 6f. This suggests that the residual stresses have been increased in the AlN/Cu joints produced at 860 ^{o}C (by comparison with those in the samples produced at 850 ^{o}C), which is reflected in the reduction of the shear strength values of these samples (Fig. 5)

The microstructure at the ceramic/metal interface was thoroughly investigated as well, in order to cast light on the influence of brazing temperature on the shear strength of the produced AlN/Cu joints. The X-ray diffractograms recorded from the interfacial reaction zones (i.e. between the AlN ceramic and the brazing-filler metal) of samples produced at the investigated temperatures are plotted in Fig. 7. It is observed that the brazing temperature significantly affects the phase assembly developed at the interface. More specifically, the intensity of the characteristic peak of $CuAlO_2$ at $2\theta = 31.6^{o}$ (see also the right-hand side magnification in Fig. 7) is decreased with the increase of brazing temperature. This is attributed to the decomposition of $CuAlO_2$ to Cu, Al_2O_3, and O_2 under vacuum:

$$4\ CuAlO_2 \rightarrow 2\ Al_2O_3 + 4\ Cu + O_2 \uparrow \qquad (9)$$

At 860 ^{o}C, $CuAlO_2$ is completely decomposed. The presence of Ag and Cu is ascribed to the incomplete chemical etching, and the observed AgCl is the product of the reaction between $FeCl_3$ and Ag that took place during the chemical etching.

In the light of the results for the bonding strength (Fig. 5) and the above findings from the X-ray diffraction analysis (Fig. 7), it can be suggested that the increase of brazing temperature favors the

production of Cu atoms by the decomposition of $CuAlO_2$, which are then embedded in the interfacial reaction zone. Additionally, it also favors the diffusion of Ag atoms into the interfacial reaction zone, allowing them to be combined with Cu. As a result, the bonding strength between the filler metal and the interfacial reaction zone is improved.

The microstructure of the interfacial zone of AlN/Cu joints, prepared at various brazing temperatures in the range of 810 - 860 ^{o}C for 10 min, is illustrated in Fig. 8, at lower (left-hand side SEM images) and higher magnification (right-hand side SEM images). The eutectic structure of α phase (copper-based solid-solution) and α+β (silver-based solid-solution) phases is observed in the interfacial zone of the samples brazed in all the investigated temperatures. This finding suggests that the porous Cu placed on the AlN-ceramic surface should favor the nucleation of α-phase crystals. Therefore, spherical α phase is distributed in the network of the Ag-Cu eutectic structure, as shown in Figs. 8a and 8b (at both magnifications). Careful observation reveals the presence of holes and cracks at the interface with the filler.

At higher brazing temperatures, the spherical α phase is gradually growing in size. Meanwhile, the network structure of the Ag-Cu eutectic is maintained, but its amount is decreased gradually with the rise of temperature, as illustrated in Figs. 8c, 8d, and 8e. According to the Ag-Cu phase diagram [30], the solubility of Cu in the liquid phase is increased with the increase of temperature. Thus, in the presence of the Ag foil, more copper atoms from the porous Cu layer and the Cu plate are dissolved in the liquid phase when the brazing temperature increases. Hence, the α phase crystallizes and grows in the undissolved porous Cu layer and the Cu plate, resulting in the growth of spherical α phase and in the decrease of the Ag-Cu eutectic phase.

When the brazing temperature reaches 860 ^{o}C, the AlN/Cu joint is totally comprised of α phase, while the network of the Ag-Cu eutectic disappears, as depicted in Fig. 8f. This microstructure results in the decline of the AlN/Cu joint strength (Fig. 5). Consequently, it is suggested that the Ag-Cu eutectic network formed, has a beneficial effect on the reduction of the residual stresses at the interfacial zone of the AlN/Cu joints [31]. Accordingly, the shear strength of the AlN/Cu joints reaches the peak value of 48.5 MPa when the brazing temperature is at 850 ^{o}C, as presented in Figs. 5 and 8e.

3.3 Mechanism of the evolution of the interfacial microstructure of the AlN/Cu joints

The study of the kinetics is the means of throwing light on the mechanism of the reaction that takes place at the investigated ceramic/metal interface. The evolution of the microstructure of the interfacial zone (cross-section) of AlN(Cu)/Ag/Cu joint assembly brazed at 785 ^{o}C over brazing time is shown in Fig. 9. This temperature was selected because, according to the Ag-Cu phase diagram, the eutectic temperature of the Ag-Cu eutectic composition, which is $Ag_{72}Cu_{28}$, is 780 ^{o}C [30].

When the soaking time is zero, the Ag foil is only in local contact with the porous Cu layer deposited on the surface of the AlN ceramic. There is no evidence of an obvious reaction at the interface (Fig. 9a). After

2 min, the Ag foil begins to react with the porous Cu layer on the surface of the AlN ceramic, and it is diffused inwards, along the channels in the porous Cu layer, resulting in bright-white β phase, formed in the porous Cu layer (Fig. 9b).

When the brazing time is prolonged, the Ag foil gradually diffuses into the porous Cu layer, and forms Ag-Cu eutectic liquid phase in the channels. This favors the densification of the porous Cu layer. Finally, the Ag-Cu eutectic appears on the walls of the pores, and spherical α phase appears in the channels, as illustrated in Figs. 9c and 9d. Nevertheless, when the brazing time is longer that 10 min, the higher amount of Cu dissolved in the Ag-Cu eutectic liquid should lead to a decrease of the number of the nuclei of α phase. During the cooling of these samples (i.e. those produced at prolonged brazing times), the pre-eutectic α phase crystallizes on the undissolved Cu matrix. This leads to the growth of the spherical α phase, and the liquid phase of the eutectic component crystallizes in the form of α+β eutectic structure, as depicted in Figs. 9e and 9f.

According to the experimental results of the present study, the bonding mechanism of AlN ceramics with a Cu plate using Ag foil as a brazing-filler metal, which is schematically summarized in Fig. 10, is suggested. More specifically, when the brazing process to produce the AlN/Cu joint starts, the porous Cu layer deposited on the surface of the AlN ceramic, the Ag foil, and the Cu plate are in close contact to one another (Fig. 10a). With the increase of brazing temperature and time, this intimate-contact configuration favors the Ag atoms to diffuse into the porous Cu layer (Fig. 10b) and the Cu plate to form Ag-Cu eutectic liquid phase (Fig. 10c).

The Ag-Cu eutectic liquid phase is formed at the sidewalls of the porous Cu and it will rapidly fill the pores of the Cu layer on account of capillary effect (Fig. 10d). Meanwhile, the Ag-Cu eutectic liquid phase is also formed on the Cu-plate side and it will favor the joining with the Cu plate. In prolonged brazing times, all the Ag foil should completely react to form Ag-Cu eutectic liquid. Furthermore, part of the porous Cu layer and the Cu plate should be dissolved in the Ag-Cu eutectic liquid phase.

During the cooling of the brazing-filler metal, supersaturated copper in the liquid phase precipitates to form spherical α phase, where the undissolved porous copper acts as nuclei of crystallization (Fig. 10e). Finally, the Ag-Cu eutectic ($Ag_{72}Cu_{28}$) precipitates in the residual liquid while the composition reaches the eutectic one. After the brazing process is finished, the microstructure of the AlN (Cu)/Ag/Cu joints is comprised of spherical α phase and Ag-Cu eutectic, distributed in the spherical α phase (Fig. 10f). Moreover, the Cu atoms produced from the decomposition of $CuAlO_2$ in the interfacial reaction zone form the tiny punctuate phase distributed in the α phase

4. Conclusions

1. A network of porous Cu layer was deposited on the surface of AlN ceramics by thick-film metallization method. The final assembly of the microstructure on the surface of the ceramic is network-porous-Cu layer / $CuAlO_2 + Al_2O_3$ / AlN.

2. Using Ag foil as brazing-filler metal, AlN(Cu) and Cu were bonded successfully. The assembly of the microstructure of the joint is Cu / Ag(s) + Cu(s) / $CuAlO_2$ + Al_2O_3 + Cu(s) / AlN. The strength of the AlN/Cu joint reached the maximum value of 48.5 MPa after brazing at 850 ^oC for 10 min. This is attributed to the above microstructure, which should effectively reduce the residual stresses at the interfacial reaction zone and improve the joint strength.
3. The successful bonding of the AlN/Cu joints by the new brazing method is ascribed to the formation of Ag-Cu eutectic liquid, which fills the pores of the network of the porous-Cu layer. The network microstructure with spherical α phase and a small amount of Ag-Cu eutectic favors the strong bonding of AlN/Cu joints.

Declarations

Acknowledgement

This work was supported by the Department of Education's Production-Study-Research combined with the innovation Funding "Blue fire plan (Huizhou)" [No. CXZJHZ201733]

References

[1] J. He, T. Zhao, J. Xin and N. Demerdash, International Conference on Renewable Energy Research and Application, IEEE (2015) https://doi.org/10.1109/ICRERA.2014.7016485.

[2] A. Morya, M. Moosavi, M.C. Gardner and H.A. Toliyat, International Electric Machines and Drives Conference (IEMDC), IEEE (2017) https://doi.org/10.1109/IEMDC.2017.8002288.

[3] K.C. Reinhardt and M.A. Marciniak, IECEC 96. Proceedings of the 31st Intersociety Energy Conversion Engineering Conference, IEE (1996) https://doi.org/10.1109/IECEC.1996.552858.

[4] M. Hoshi, 2016 28th International Symposium on Power Semiconductor Devices and ICs (ISPSD), Prague (2016) https://doi.org/10.1109/ISPSD.2016.7520765.

[5] J. Barcena, J. Maudes, M. Vellvehi, X. Jorda, I. Obieta, C. Guraya, L. Bilbao, C. Jimenez, C. Merveille, J. Coleto, Acta Astronaut. (2008) https://doi.org/10.1016/j.actaastro.2008.01.010.

[6] J. Broughton, V. Smet, R.R Tummala, Y.K. Joshi, J. Electronic Packaging (2018) https://doi.org/10.1115/1.4040828.

[7] Z. Liang, 2015 IEEE International Workshop on Integrated Power Packaging (IWIPP), IEEE (2015) https://doi.org/10.1109/IWIPP.2015.7295970.

[8] R. Khazaka，L. Mendizabal, D. Henry, R. Hanna, IEEE T. power Electr. (2014) https://doi.org/10.1109/TPEL.2014.2357836.

[9] B. Mouawad, C. Buttay, M. Soueidan, H. Morel, F. Mercier, 2012 24th International Symposium on Power Semiconductor Devices and ICs, Bruges (2012) https://doi.org/doi: 10.1109/ISPSD.2012.6229081.

[10] K. Hromadka, J. Stulik, J. Reboun, A. Hamacek, Procedia Engineering (2014) https://doi.org/10.1016/j.proeng.2014.03.107.

[11] J. Hlina, J. Reboun, A. Hamacek, Scripta Mater. (2020) https://doi.org/10.1016/j.scriptamat.2019.09.029.

[12] J. Schulz-Harder, Twenty-Second Annual IEEE Semiconductor Thermal Measurement And Management Symposium, IEEE (2006) https://doi.org/10.1109/STHERM.2006.1625233.

[13] S. Zhang, L. Yan, K. Gao, H. Yang, X. Wan, Ceram. Int. (2019) https://doi.org/10.1016/j.ceramint.2019.04.186.

[14] I.B. Krasniy, A.A. Denisova and S.A. Kumacheva, 2016 13th International Scientific-Technical Conference on Actual Problems of Electronics Instrument Engineering (APEIE), Novosibirsk, (2016) https://doi.org/10.1109/APEIE.2016.7807089.

[15] J. Jarrige, T. Joyeux, J.P. Lecompte, J.C. Labbe, J. Eur. Ceram. Soc. (2007) https://doi.org/10.1016/j.jeurceramsoc.2006.04.037.

[16] M. Chmielewski, Proceedings of SPIE the International Society for Optical Engineering, (2005) https://doi.org/10.1117/12.610676.

[17] A.L. Molisani, H.N. Yoshimura, Materials Science Forum scientific (2010) https://doi.org/10.4028/www.scientific.net/MSF.660-661.658.

[18] B. Kabaar, A.C. Buttay, O. Dezellus, R. Estevez, A. Gravouil, L. Gremillard, Microelectron. Reliab. (2017) https://doi.org/10.1016/j.microrel.2017.06.001.

[19] G. Dong, C. Xu, X. Zhang, K.D.T. Ngo, G.Q. Lu, Solder. Surf. Mt. Tech. (2010) https://doi.org/info:doi/10.1108/09540911011036280.

[20] J. Shi, Q. Wang, J. Li, J. Xiong, J. Feng, Mater. Charact. (2019) https://doi.org/10.1016/j.matchar.2019.109850.

[21] Y.W. A, Z.W.Y. A, L.X.Z. B, D.P.W. A, J.C.F. B, J. Materiomics, (2016) https://doi.org/10.1016/j.jmat.2015.10.003

[22] J. Ba, X.H. Zheng, R. Ning, J.H. Lin, J.L. Qi, J. Cao, W. Cai, J.C. Feng, Ceram. Int. (2018) https://doi.org/10.1016/j.ceramint.2018.03.018.

[23] H. Xu, F. Meng, X. Lei, J. Yang, Y. Zhao, Ceram. Int. (2020) https://doi.org/10.1016/j.ceramint.2020.07.047.

[24] M. Keita, M. Tomoki, S. Tomokazu, H. Akio, J. Electron. Mater. (2018) https://doi.org/10.1007/s11664-018-6504-2.

[25] J.L. Lv, Y.L. Huang, R.L. Fu, Y.R. Ji, B.Y. Wu, X.H. Liu, J. Eur. Ceram. Soc. (2020) https://doi.org/10.1016/j.jeurceramsoc.2020.07.060.

[26] G.Z. Ren, T.C. Zhang, X.C. Wang, The reactions of CuO at high pressure and high temperature, J. Phys-Condens. Mat. (2002) https://doi.org/10.1088/0953-8984/14/44/448.

[27] A. Kara-Slimane, D. Juve, E. Leblond, D. Treheux, J. Eur. Ceram. Soc. (2000) https://doi.org/10.1016/S0955-2219(00)00037-6.

[28] K.T. Jacob, C.B. Alock, J. cheminformatics (1975) https://doi.org/10.1111/j.1151-2916.1975.tb11441.x.

[29] Y.H. Huang, S.F. Wang, A.P. Tsai, S. Kameoka, Ceram. Int. (2014) https://doi.org/10.1016/j.ceramint.2013.08.130.

[30] X.W. Zuo, C.C. Zhao, L. Zhang, E.G. Wang, Materials (2016) https://doi.org/10.3390/ma9070569.

[31] G. Wang, Y.J. Cai, W. Wang, J. Manuf. Process (2019) https://doi.org/10.1016/j.jmapro.2019.03.023.

Figures

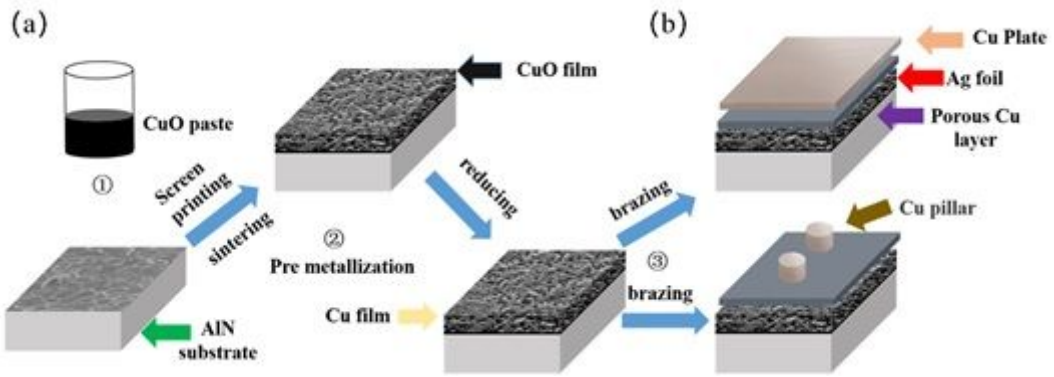

Figure 1

(a) Experimental procedure of the pre-metallization of the AlN substrate and the Cu-bonding, and (b) the brazing assembly.

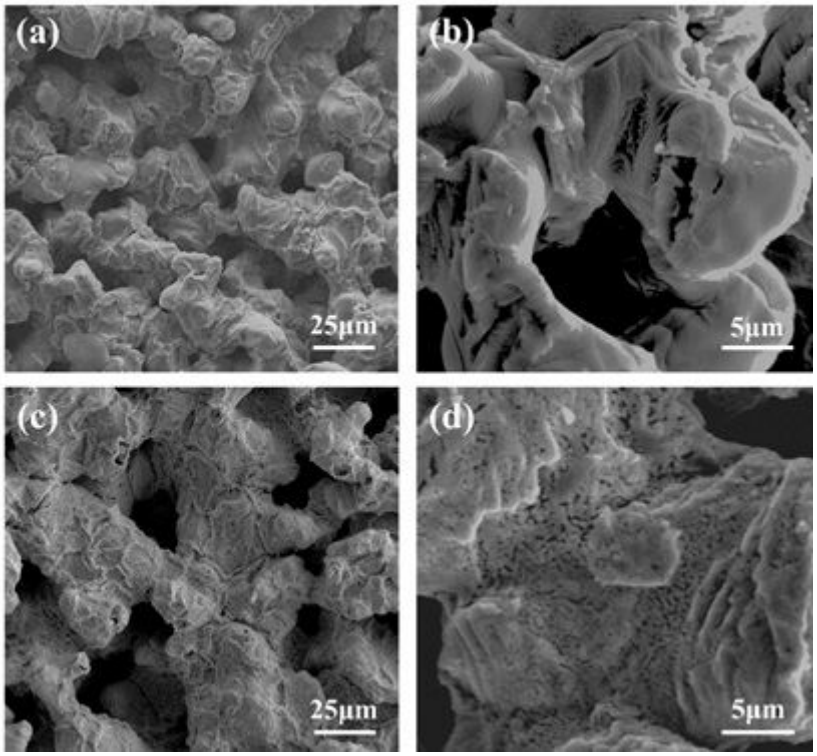

Figure 2

Morphology (top view, observed at lower and higher magnification) of the pre-metalized layer of (a-b) CuO and (c-d) Cu, deposited on the surface of the AlN-ceramic substrate by the thick-film method.

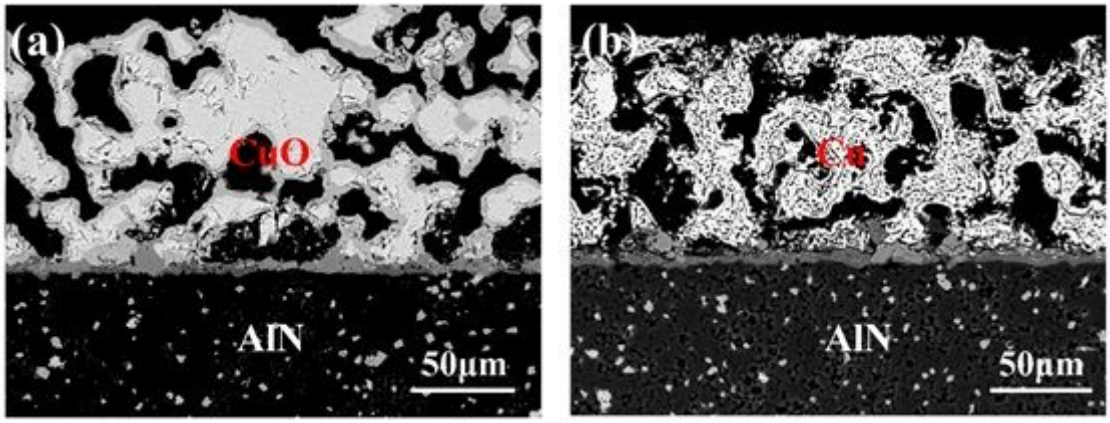

Figure 3

Cross-section of the microstructure of pre-metalized layer of (a) CuO and (b) Cu, deposited on the surface of the AlN-ceramic substrate.

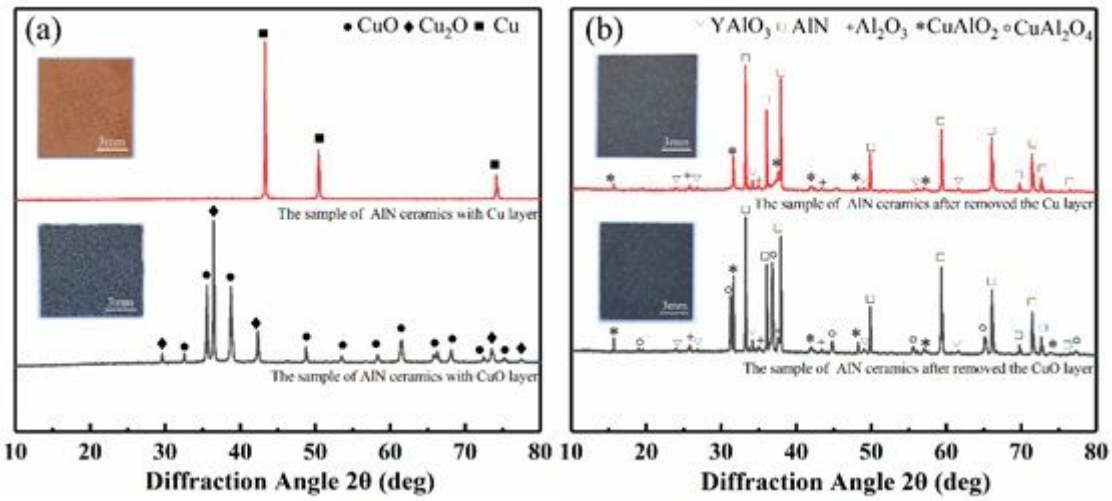

Figure 4

X-ray diffractograms (a) of the CuO layer (bottom), the Cu layer (upper) deposited on the surface of the AlN-ceramic substrate (produced after sintering at 1075 oC for 30 min), and (b) of the corresponding interfacial reaction zone revealed on the surface of the AlN-ceramic substrate after chemical etching.

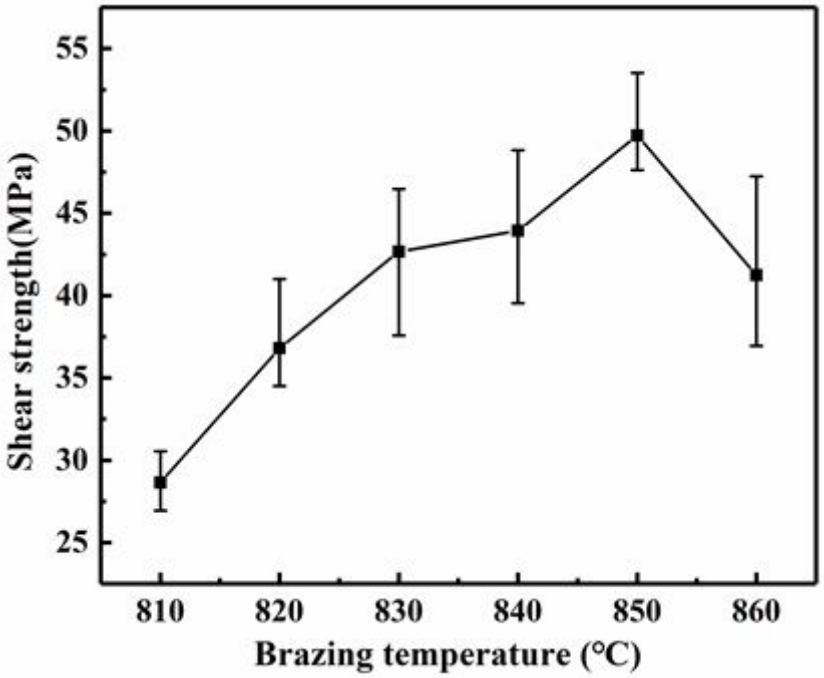

Figure 5

Influence of brazing temperature on the shear strength of the AlN/Cu joints produced after brazing for 10 min.

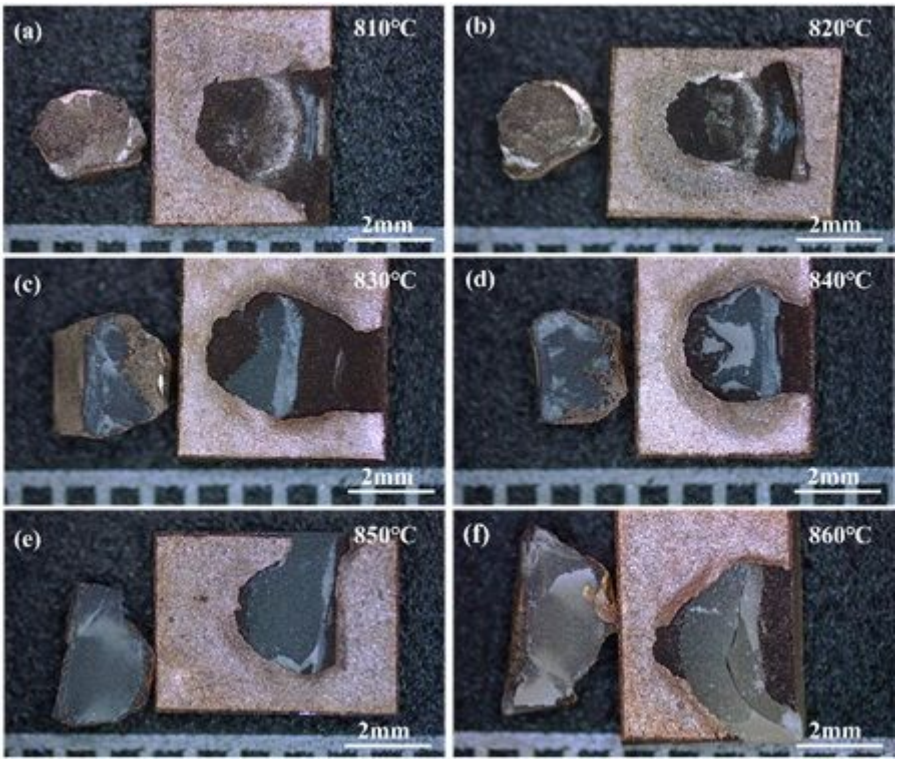

Figure 6

Images from fractography obtained from the AlN/Cu joints produced at various brazing temperatures. (The brazing time was 10 min).

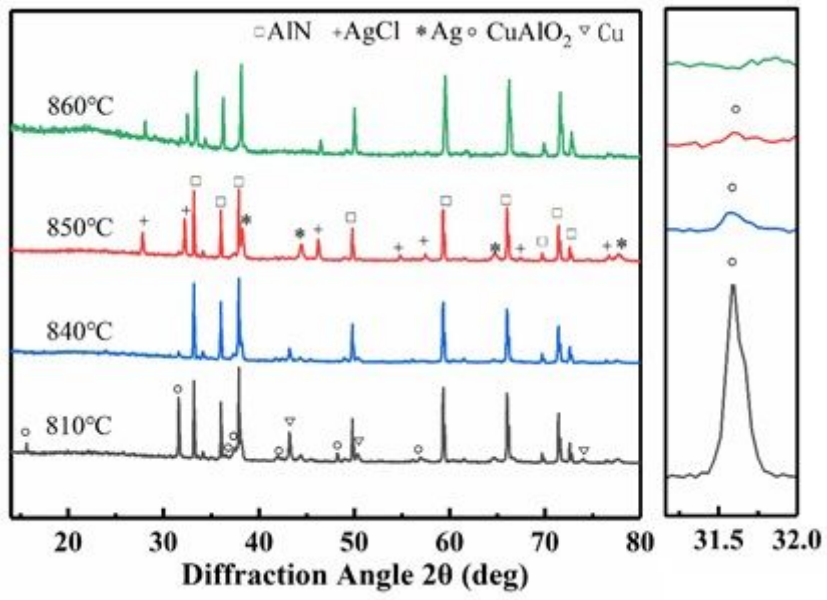

Figure 7

Influence of brazing temperature on the X-ray diffractograms recorded from the interfacial reaction zone between the AlN ceramic and the filler metal. (The brazing time was 10 min).

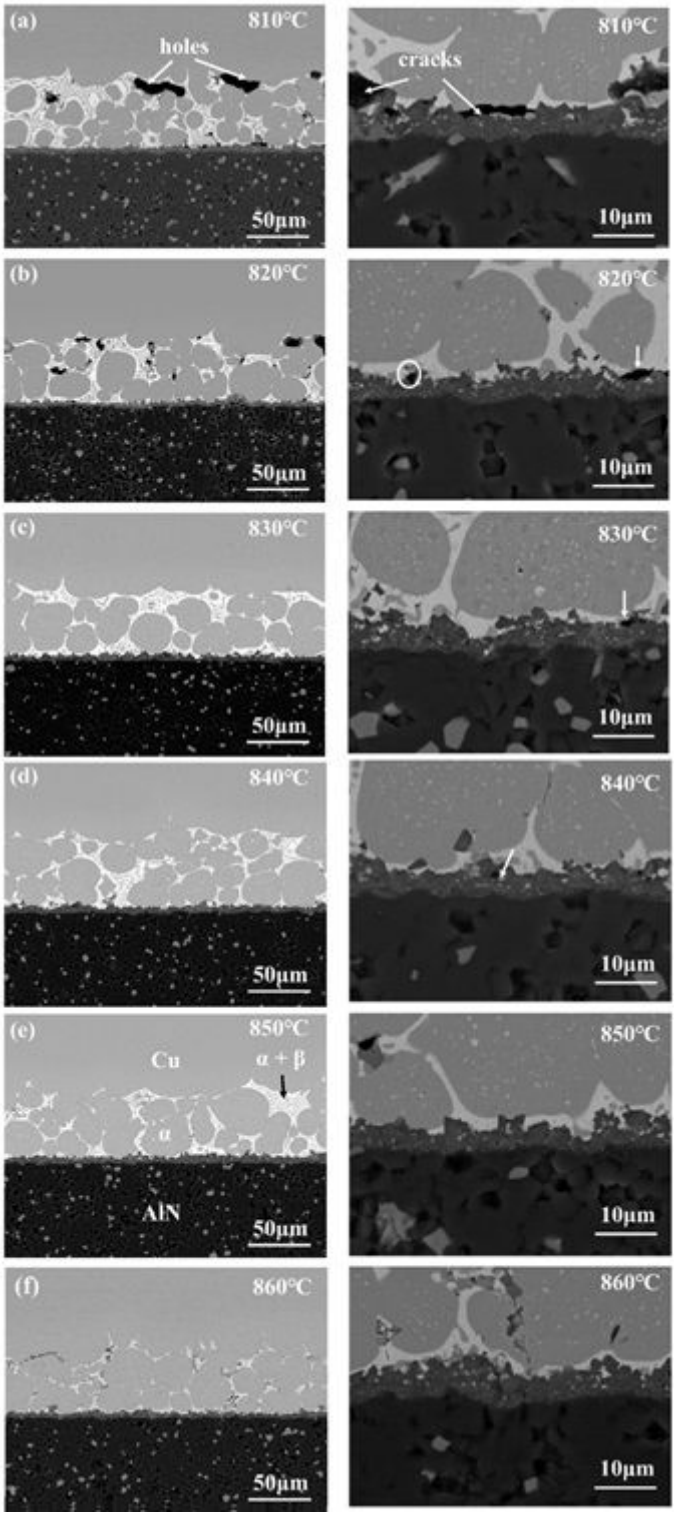

Figure 8

Influence of brazing temperature on the interfacial microstructure of the AlN/Cu joints, observed at lower (left-hand side) and higher (right-hand side) magnifications. (The brazing time was 10 min).

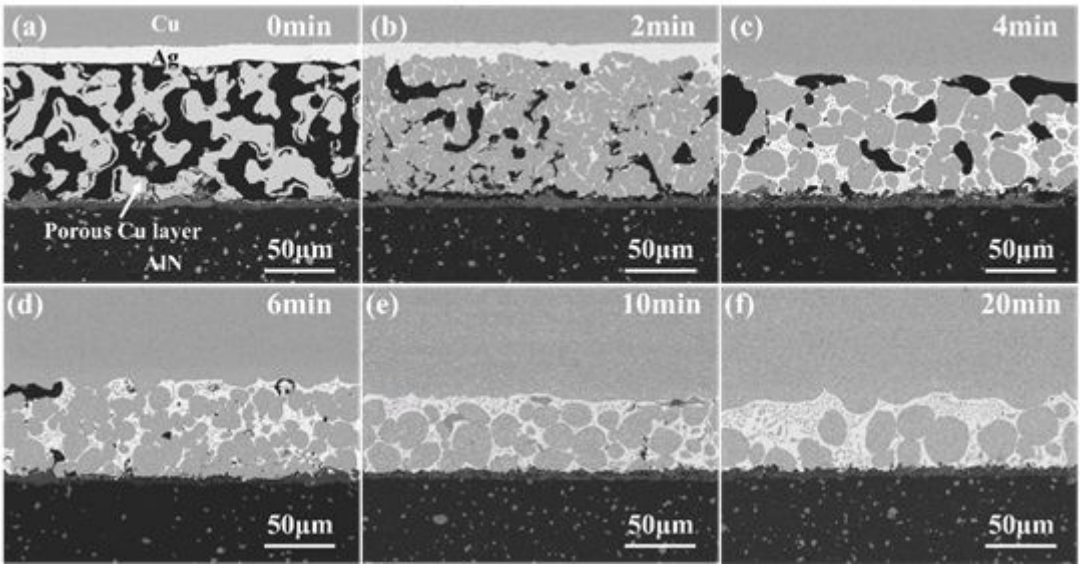

Figure 9

Influence of brazing time on the interfacial microstructure of the AlN/Cu joints. (The brazing temperature was 785 oC).

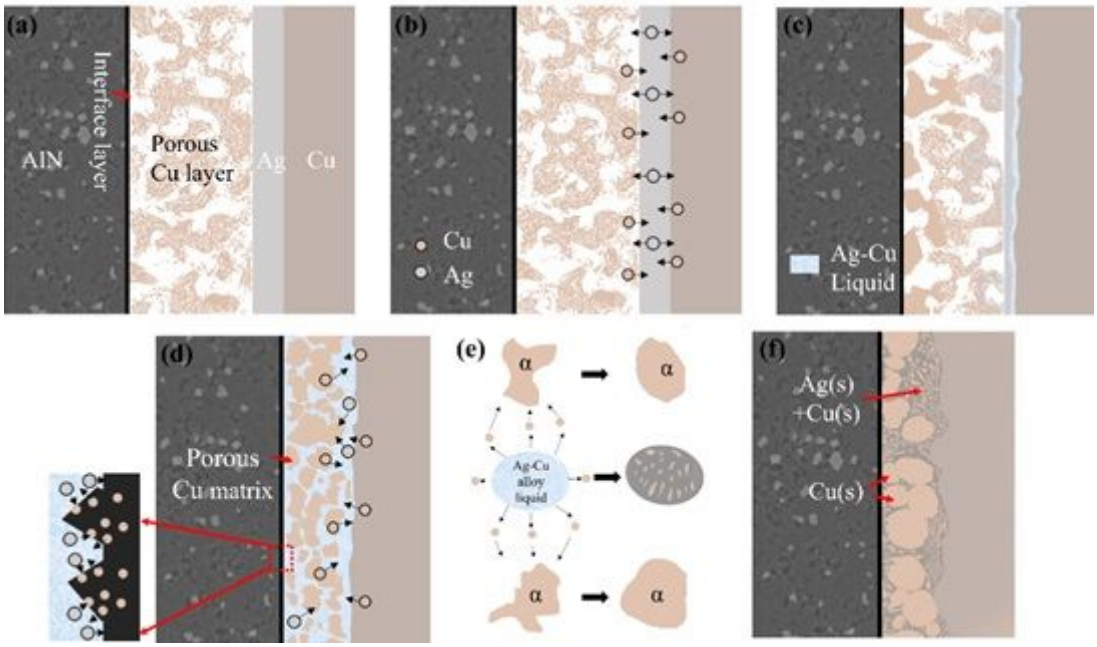

Figure 10

Schematic representation of the proposed reaction mechanism for the brazing of the AlN ceramic with the Cu plate, using porous Cu and Ag foil.